Scientific Research Publishing

Atmospheric and Climate Sciences, 2026, 16(3), 495-510
https://www.scirp.org/journal/acs
ISSN Online: 2160-0422
ISSN Print: 2160-0414

Triggering and Enhancement Mechanisms of Extreme Precipitation over the Complex Terrain in the Central Loess Plateau

Zhexi Wu, Bo Zhang*, Di An, Xueying Zhang

College of Geography and Environmental Science, Northwest Normal University, Lanzhou, China
Email: *zhangbo@nwnu.edu.cn

How to cite this paper: Wu, Z.X., Zhang, B., An, D. and Zhang, X.Y. (2026) Triggering and Enhancement Mechanisms of Extreme Precipitation over the Complex Terrain in the Central Loess Plateau. *Atmospheric and Climate Sciences*, **16**, 495-510.
https://doi.org/10.4236/acs.2026.163025

Received: November 1, 2025
Accepted: May 11, 2026
Published: May 14, 2026

Abstract

Using the WRF model, this study conducts numerical simulations to investigate the triggering and enhancement mechanisms of an extreme precipitation event over the Central Loess Plateau. By performing comparative experiments under real and smoothed terrain conditions, combined with qualitative observational validation using sparse station data and diagnostic analysis, the study reveals the physical processes responsible for the initiation of deep convection and precipitation intensification over complex terrain. The results show that the hilly and gully terrain forces the warm and moist airflow on the periphery of the subtropical high to ascend and converge, leading to a notable advancement of convective initiation by approximately two hours and a significant intensification of rainfall. Convective cells generated over multiple hills tend to converge and rapidly merge into a mesoscale convective system under the influence of the low-level wind field, resulting in a rapid expansion of precipitation intensity and coverage. The peak hourly rainfall reaches 40 - 60 mm/h under real terrain, compared with less than 20 mm/h under smoothed terrain, and the maximum accumulated rainfall increases by about 2.1 times. This study refines the understanding of the development processes of extreme precipitation under the influence of complex topography over the Loess Plateau and provides a scientific basis for improving local heavy rainfall forecasting and disaster prevention.

Keywords

Loess Plateau, Complex Terrain, Extreme Precipitation, Numerical Simulation

1. Introduction

Extreme rainstorms are often the result of interactions among multi-scale weather

systems. In China, torrential and especially extraordinary rainstorms are primarily influenced by large-scale systems such as typhoons, frontal systems, and cyclonic vortices migrating eastward from the Qinghai-Xizang Plateau and its surrounding regions. However, in certain regions where large-scale forcing is weak, local topography and mesoscale or smaller-scale systems become key factors in triggering deep convection. The heartland of the Loess Plateau is characterized by a landscape of hills and gullies, with highly fragmented terrain that favors the occurrence of localized flash rainstorms. For example, on 25 - 26 July 2017, a localized torrential rainstorm struck southern Yulin, Shaanxi Province, producing record-breaking flooding in the Wuding River since 1960 [1]. These systems are discussed here as the broader synoptic background commonly associated with heavy rainfall in the Loess Plateau, whereas the present case is examined mainly in relation to the periphery flow of the subtropical high and terrain forcing.

Many scholars have conducted diagnostic and mechanistic studies on the causes of rainstorms in northern inland China. Tao Shiyan *et al.* summarized that the main triggering systems of heavy rainfall in China include typhoon lows, quasi-stationary fronts, and plateau vortices [2]. Ding Yihui (2014) emphasized that rainstorms are the products of coupled multi-scale systems [3]. Over the Loess Plateau and its transitional zones, the Hetao vortex is one of the major systems influencing summer rainstorms [4]. Zhang Hong *et al.* (2006) analyzed a heavy rainfall process in northern Shaanxi and found that the combined effects of a distant typhoon circulation and the Hetao vortex could repeatedly trigger mesoscale convective systems in the rainstorm region, leading to sudden extreme rainfall [5]. Wang Weitai *et al.* (2009) showed that during its development, the Hetao vortex exhibits an unstable "warm-below, cold-above" structure, and the superposition of upper-level positive vorticity favors the induction of intense precipitation [6]. Liang Feng and Tao Shiyan (2007) proposed that when the Hetao cyclone intensifies rapidly, multiple mesoscale convective systems often align to its northwest, collectively producing widespread heavy rainfall [7].

In addition, the position and strength of the subtropical high play a regulatory role in regional rainstorms. When the Western Pacific Subtropical High extends anomalously westward, a pattern of a southwesterly low-level jet at 700 hPa intersecting with a southeasterly low-level jet at 850 hPa tends to form along its periphery, transporting abundant moisture into the rainstorm region. The nocturnal intensification of the low-level jet often gives rise to night-time-peaking rainstorms [8]. Liu Yong *et al.* (2006) found through case analysis that the establishment of a low-level jet plays a crucial role in major rainstorms over the Loess Plateau [9], while low- and mid-level jets have been widely recognized as a key dynamical precursor for the initiation and maintenance of heavy rainfall systems over China [10]. Low-level jets not only transport moisture but also enhance low-level convergence and orographic uplift, thereby facilitating the initiation and development of convection systems [11]. Liu Hongbo *et al.* (2014), in their review of low-level jet studies, pointed out that most low-level jets are accompanied by

strong precipitation events such as rainstorms [12].

Beyond the large-scale background, topographic factors are also regarded as key in triggering rainstorms over northern Shaanxi and adjacent areas. The southern Loess Plateau is a typical hilly-gully region with deeply incised terrain and elevation differences of several hundred meters. Through thermal forcing and dynamical lifting, such complex topography can induce local convection even under weak synoptic forcing. Many warm-sector rainstorms occur when warm and moist airflow interacts with terrain in the absence of obvious frontal systems [13]. In addition, multi-scale perturbations associated with upstream low-level vortices can act as triggering "seeds" for mesoscale convective systems. For example, the 21 July 2012 Beijing extreme rainstorm exhibited a self-organized convective system initiated by upstream vortex disturbances, with a long-lived structure exceeding 40 hours [14]. Jing Xi *et al.* (2013) analyzed a sudden rainstorm event over the Loess Plateau and revealed a characteristic vertical circulation structure: β-mesoscale cyclonic convergence at low levels coupled with strong upper-level divergence, which triggered and maintained vigorous deep convection [15]. Collectively, these studies have revealed the causes of rainstorms over the Loess Plateau and surrounding regions from both synoptic and mesoscale perspectives.

Nevertheless, the specific physical roles of hilly-gully terrain in the initiation and enhancement of convection remain insufficiently understood. Questions such as how small-scale topographic undulations trigger multiple convective cells, and why these cells tend to merge into stronger precipitation systems, still lack systematic answers. To address these key scientific gaps, this study employs numerical simulations and diagnostic analyses to investigate an extreme precipitation event over the Loess Plateau, aiming to elucidate its triggering and enhancement mechanisms and to supplement the limitations of traditional observational analyses. In this study, these broader systems are treated as the background environment, while the analysis concentrates on the terrain-induced triggering and organization of convection in the target event.

2. Study Area and Data

2.1. Study Area

The study area is located in the central-southern Loess Plateau (34˚ - 41˚N, 102˚ - 114˚E), characterized by a landscape of hills and gullies. The region is dominated by loess-covered residual plateaus and deeply incised valleys, with elevations ranging from 800 to 1500 m. The terrain is highly dissected and exhibits strong topographic relief (**Figure 1**). This area belongs to a typical continental monsoon climate zone, with an annual mean precipitation of about 500 - 600 mm, over 70% of which occurs from July to September, when heavy rainstorms are frequent. The annual mean temperature ranges from 8˚C - 12˚C in the south to 5˚C - 8˚C in the north, while potential evapotranspiration reaches 800 - 1000 mm [16], leading to a pronounced imbalance between water supply and energy availability.

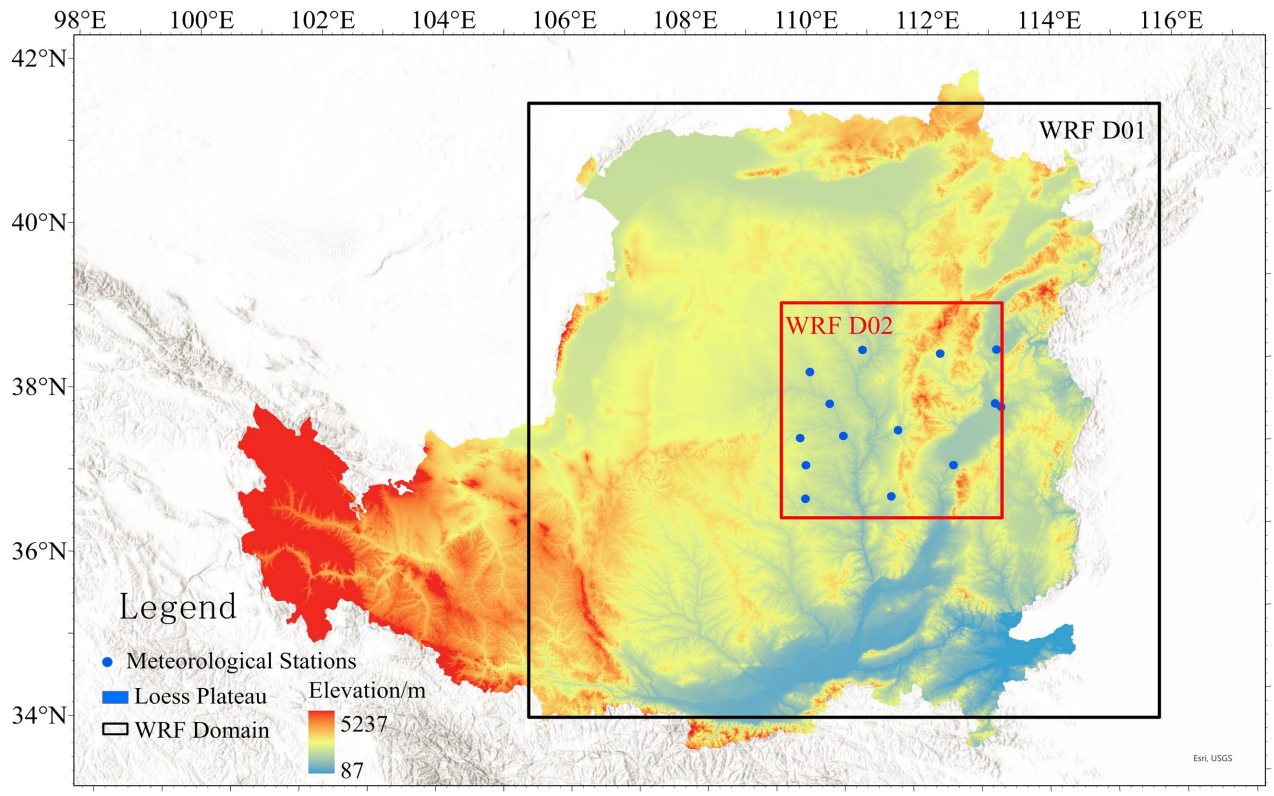

Figure 1. Location of the study area.

The Yellow River and its major tributaries, including the Wei River and Fen River, flow through this region. Due to the loose soil structure and sparse vegetation cover, extreme precipitation events often lead not only to flooding but also to secondary geological hazards such as landslides and debris flows, making the area one of the most disaster-prone regions in China for soil erosion and flash floods. Moreover, the complex exchanges of heat and moisture within the boundary layer make the Loess Plateau not only highly sensitive to climate change but also a hotspot for local severe convective storms [17].

2.2. Data

The initial and boundary conditions for the WRF numerical simulations were derived from two datasets: the NCEP FNL global analysis data (https://www.ncep.noaa.gov) and the ERA5-Land reanalysis data (https://cds.climate.copernicus.eu). The FNL analysis provides large-scale atmospheric circulation backgrounds with a horizontal resolution of 1˚ × 1˚, available every six hours, including wind, temperature, humidity, and pressure fields at multiple atmospheric levels. The ERA5-Land dataset offers high-resolution land surface information at 0.1˚ × 0.1˚ and hourly intervals, providing detailed variables such as soil moisture and surface fluxes. The topographic data were obtained from the Copernicus Digital Elevation Model released by the European Space Agency (https://spacedata.copernicus.eu), which has a spatial resolution of 30 m

and was generated through TanDEM-X interferometric radar measurements, ensuring comprehensive coverage and high accuracy.

Hourly precipitation observations from automatic weather stations were obtained from the National Meteorological Information Center of the China Meteorological Administration (http://data.cma.cn). These observations were used to qualitatively validate the temporal and spatial evolution of simulated precipitation events. Considering the relatively sparse distribution of meteorological stations across the study area—and the lack of effective observations in some regions of intense rainfall—the station data were mainly employed for qualitative comparisons of the simulated rainfall centers, timing, and temporal evolution trends, rather than for systematic quantitative error assessments.

To compensate for the limitations caused by the sparse ground-based network, this study also utilized the IMERG Final Run satellite precipitation product from NASA's Global Precipitation Measurement mission (https://gpm.nasa.gov/data/imerg). The IMERG data provide 30-minute temporal resolution and 0.1 spatial resolution, enabling detailed evaluation of the rainfall intensity and spatial distribution simulated by the WRF model.

3. Model and Experimental Design

3.1. WRF Model Design

This study employed version 4.6 of the Weather Research and Forecasting model. According to the domain frame shown in **Figure 1**, the parent domain (D01) extended approximately from 34.0˚N to 41.5˚N and from 105.5˚E to 114.8˚E, while the nested domain (D02) extended approximately from 36.4˚N to 38.9˚N and from 108.6˚E to 112.1˚E. The simulation domain adopted a two-way nested configuration: the parent domain (D01) covered most of the Loess Plateau and surrounding regions, with a grid size of 241 × 211, while the nested domain (D02) focused on the central and eastern hilly-gully region of the Plateau, with a horizontal resolution of 3 km and a grid size of 301 × 301. Both domains contained 50 vertical σ-levels, with the model top set at 50 hPa.

In terms of physical parameterization schemes, based on previous experimental results over the Loess Plateau [18] and preliminary multi-scheme sensitivity tests, a configuration known for stable regional performance was selected. This configuration was chosen because it has shown robust performance in Loess Plateau precipitation simulations, especially in reproducing terrain-induced convection while maintaining a reasonable computational cost. The Grell-Freitas cumulus scheme was used for D01, while no cumulus parameterization was applied in D02 due to its convection-permitting resolution (3 km). The Thompson microphysics scheme was adopted to represent ice-phase processes. The YSU (Yonsei University) planetary boundary layer scheme was used with a non-local mixing approach, the Monin-Obukhov surface layer scheme for surface flux parameterization, and the Noah-LSM land surface model for land-atmosphere interactions. For radiative processes, the RRTMG schemes were applied for both longwave and shortwave

radiation [19].

Two parallel experiments were designed on this basis: the real-terrain experiment and the smoothed-terrain experiment (**Figure 2**). The real-terrain experiment utilized the original high-resolution topographic data, fully preserving the natural hilly and gully undulations. The smoothed-terrain experiment, by contrast, involved topographic smoothing to reduce mesoscale variations. Specifically, during the WRF Preprocessing System stage, the DEM data were subjected to multiple passes of nine-point smoothing, effectively diminishing terrain fluctuations smaller than 30 km, while retaining the large-scale terrain configuration. After smoothing, the surface elevation difference within the D02 domain was reduced from approximately 800 m to less than 200 m, yielding an approximately flat terrain field that still preserved the broad regional slope pattern [20].

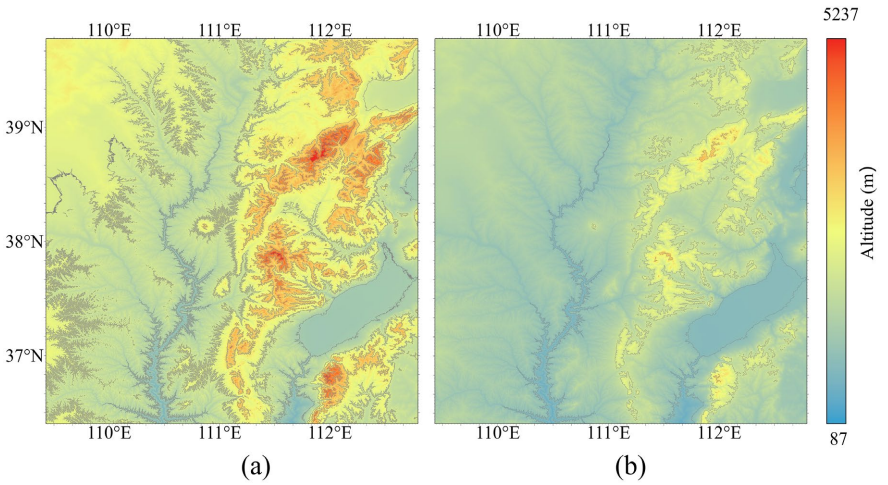

Figure 2. Terrain schematic for WRF model domain D02: (a) Real-terrain experiment; (b) Smoothed-terrain experiment.

Apart from the difference in terrain, the two experiments shared identical initial conditions and parameter settings. The simulation was initialized at 00:00 Beijing Time on 14 July 2022 (all times hereafter are in Beijing Time) and integrated until 00:00 on 16 July, fully encompassing the entire evolution of the rainstorm event. To minimize the influence of the model spin-up period, the analysis primarily focused on the intense precipitation stage from 08:00 on 15 July to 02:00 on 16 July.

To ensure consistency of the large-scale atmospheric background between the two experiments, a weak Four-Dimensional Data Assimilation nudging term was introduced during the integration of the smoothed-terrain experiment. This approach constrained its large-scale circulation evolution to remain close to that of the real-terrain simulation, while allowing mesoscale and smaller-scale features to develop freely. Such an experimental design concept is analogous to the "terrain replacement" method, which has been widely used in previous studies to assess the contribution of topography to precipitation formation [21].

3.2. Diagnostic Methods

To comprehensively analyze the mechanisms by which terrain triggers and enhances extreme precipitation, this study selected key diagnostic variables from three aspects: moisture transport, dynamic lifting, and atmospheric instability [22]. The core indicators and their definitions are as follows:

1) Vertically Integrated Moisture Flux Convergence (VIMFC): This parameter measures the intensity of horizontal moisture convergence within the entire atmospheric column and is defined as:

$$\mathrm{VIMFC} = -\frac{1}{g}\nabla \cdot \int_{p_s}^{300\,\mathrm{hPa}} q\,V\,\mathrm{d}p \tag{1}$$

where q is the specific humidity, V is the horizontal wind vector (m/s), and g is the gravitational acceleration (9.8 m/s^2). The integration extends from the surface pressure to 300 hPa. A negative VIMFC value indicates moisture convergence, and the larger its absolute value, the stronger the moisture accumulation per unit area, which is more favorable for the development of deep convection. This study particularly focuses on the 850 hPa moisture convergence field to characterize the modulating effect of terrain on low-level moist zones.

2) Vertical Velocity (w): This variable reflects the intensity of terrain-induced vertical motion and is taken directly from the model's vertical velocity output (m/s). Its physical expression is:

$$w = -\frac{1}{\rho g}\cdot\frac{\mathrm{d}p}{\mathrm{d}t} \tag{2}$$

where ρ is the air density, is the gravitational acceleration, and $\frac{\mathrm{d}p}{\mathrm{d}t}$ represents the pressure tendency. The analysis focuses on the vertical velocity field between 2 - 5 km above ground level, comparing the real-terrain and smoothed-terrain experiments to identify whether hilly terrain induces localized forced uplift.

3) Convective Available Potential Energy (CAPE): CAPE is widely used in extreme precipitation studies to quantify atmospheric instability and the potential intensity of convection. It is calculated as:

$$\mathrm{CAPE} = \int_{z_{\mathrm{LFC}}}^{z_{\mathrm{EL}}} g\frac{T_{v,p} - T_{v,e}}{T_{v,e}}\mathrm{d}z \tag{3}$$

where z_{EL} is the level of free convection, z_{LFC} is the equilibrium level, g is the gravitational acceleration (9.8 m/s^2), $T_{v,p}$ is the virtual temperature of the lifted parcel, and $T_{v,e}$ is the environmental virtual temperature. An increase in CAPE and its earlier establishment in the lower atmosphere generally indicate that convection is more easily triggered and develops more vigorously [23]. By analyzing the spatial-temporal differences of CAPE between the real-terrain and smoothed-terrain simulations, this study reveals whether the complex terrain facilitates the early release of convective instability energy, thereby enhancing convective development.

4. Results and Analysis

4.1. Spatiotemporal Distribution of Simulated Precipitation

The WRF model successfully reproduced the overall rainfall pattern of this extreme precipitation event. Figure 3(a) shows the simulated cumulative precipitation from 08:00 on 15 July to 02:00 on 16 July 2022 in the real-terrain experiment. A pro-nounced rainstorm center developed over the southwestern part of the core study area, with a maximum accumulated precipitation of about 152.8 mm, closely matching the observed value at the Ansai station (143.7 mm). The main rainband exhibited a south-west-northeast orientation, aligning with the windward slopes of hills at elevations between 1000 and 1200 m, indicating a clear influence of terrain orientation on rainfall distribution.

In addition, a secondary rainfall center appeared on the western side of the main rainband, located in the upper valley of the Jing River. The model simulated 284.3 mm of precipitation there, compared to an observed 369.2 mm, capturing the high-intensity rainfall pattern reasonably well.

In contrast, the smoothed-terrain experiment produced markedly weaker and more confined precipitation. As shown in Figure 3(b), after terrain smoothing, the maximum rainfall in the southwestern part of the study area decreased to only about 74.6 mm, less than half of that in the real-terrain case. The secondary rainfall center nearly disappeared, leaving only scattered moderate to light rainfall. This demonstrates the significant role of topography in the formation of the main rainstorm center.

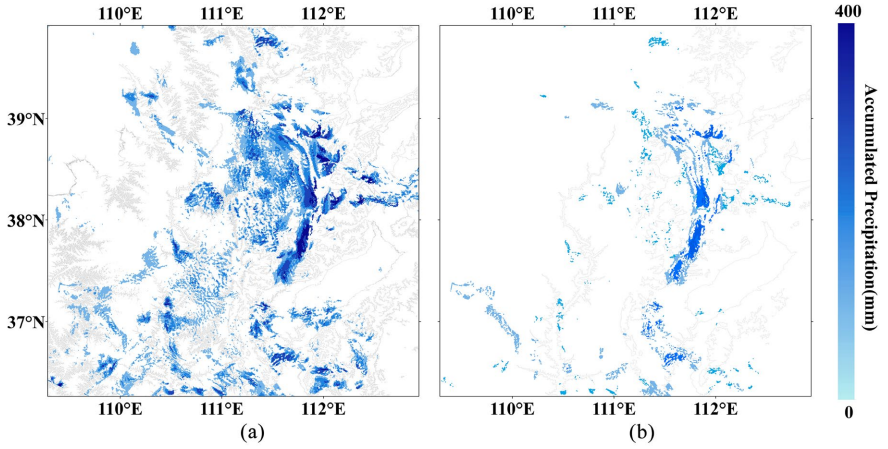

Figure 3. Spatial distribution of cumulative precipitation (mm) simulated by WRF: (a) Real-terrain experiment; (b) Smoothed-terrain experiment.

Overall, precipitation in the real-terrain experiment increased by more than 100% relative to the smoothed-terrain case over the hilly regions of Ansai and Qingcheng. The zones of high terrain-induced precipitation enhancement corresponded closely to the major gullies and mountain ridges, whereas under flat terrain conditions, convective activity weakened substantially and became spatially dispersed.

From a temporal perspective (Figure 4), the real-terrain simulation reproduced the observed evolution of the rainstorm well, with intense precipitation mainly occurring from the night of July 15 to the early morning of July 16. Taking the storm center grid point (36.86˚N, 111.54˚E) as an example, precipitation remained weak before 20:00 on July 15, followed by short-duration heavy rainfall beginning around 21:00, and a rapid intensification at 22:00, when the hourly rainfall peaked at 49.7 mm. The heavy rainfall persisted until around 01:00 on July 16. In the simulation, this explosive rainfall process resulted from the successive merging of multiple convective cells, leading to a rapid enhancement of hourly precipitation intensity.

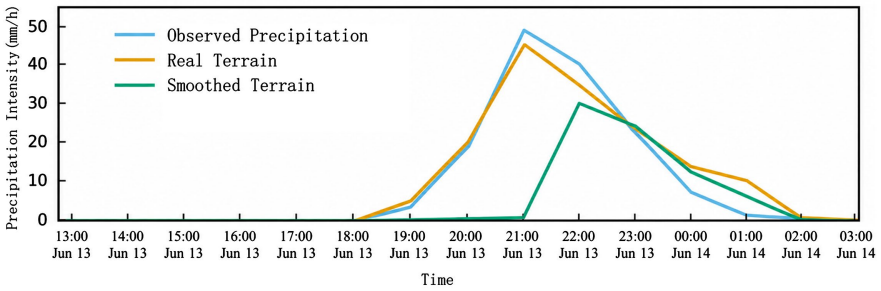

Figure 4. Comparison of hourly precipitation intensity (mm/h) near the storm center (37.86˚N, 111.54˚E).

In contrast, in the smoothed-terrain experiment, significant rainfall at the corresponding grid point did not occur until 23:00 on July 15, with a peak intensity of only about 10 mm/h. This indicates that real terrain induced an earlier and stronger convective initiation. Particularly between 21:00 and 22:00, the rainfall growth rate under real terrain was several times greater than that under smoothed terrain, confirming that terrain-triggered convective cells merged during this period, causing a burst-like intensification of precipitation. Throughout the entire storm event, the domain-averaged precipitation under real terrain was about 60% higher than that of the smoothed-terrain case, and the grid points near the Ansai center exhibited increases exceeding 120%, demonstrating an extremely significant terrain effect.

4.2. Mechanism of Terrain-Triggered Convection

To investigate the role of the hilly-gully terrain in the initial triggering of convection, the effects of topography on low-level convergence and vertical motion were analyzed. Figure 5(a) presents the vertical cross-section of wind speed across the storm center along an north-south transect at 21:00 in the real-terrain experiment. A distinct updraft is observed near the slope of the terrain, with a maximum vertical velocity exceeding 3 m/s, extending upward to a height of about 6 km. The updraft is located above the crest of a hill, indicating that terrain forcing is its primary cause. On the eastern flank of this updraft, a secondary radial downdraft branch appears between 3 - 5 km, suggesting that the main updraft has entered a

mature stage. Such a near-mountain vertical circulation structure demonstrates that terrain-induced lifting releases convective instability energy, thereby triggering deep convection.

In contrast, the smoothed-terrain experiment (**Figure 5(b)**) lacks this forced uplift near hilltops. The vertical velocity across the entire layer at 21:00 remains below 1 m/s, showing only weak and uniform ascent insufficient to surpass the level of free convection. This directly delays the onset of convection and weakens its intensity.

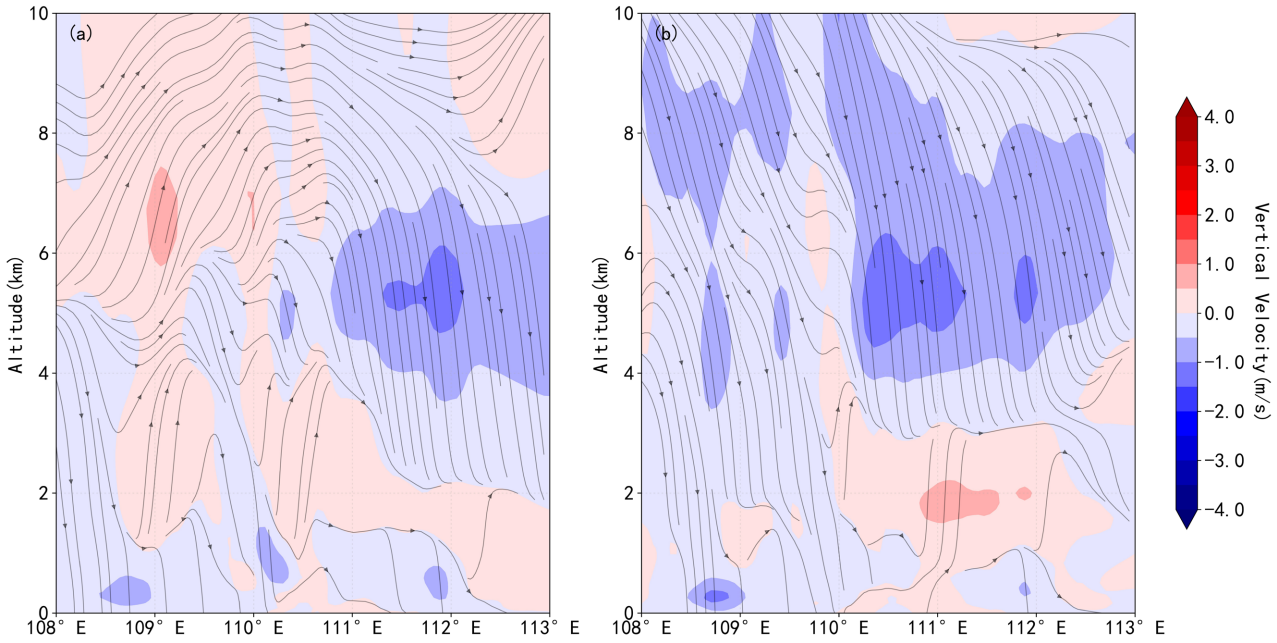

Figure 5. Vertical cross-section of wind direction and vertical velocity along the north-south axis through the storm center: (a) Real-terrain experiment; (b) Smoothed-terrain experiment.

Figure 6(a) shows the 850 hPa wind field and moisture flux at 20:00 on July 15 in the real-terrain experiment. Prior to the onset of the main rainstorm, the large-scale environment featured prevailing southerly flow, with a prominent northward moisture flux at 850 hPa. Along the windward slopes of the Loess hills, roughly near 109˚ E, a distinct moisture tongue and convergence zone developed, as indicated by the blue shading representing strong convergence. Local southerly winds encountered terrain uplift and convergence in this zone, substantially enhancing vertical motion. Notably, these windward-slope convergence belts correspond closely to the initial convection-triggering locations between 21:00 and 22:00. This confirms that the hilly terrain guided low-level airflow convergence, providing the necessary moist and ascending conditions for convective initiation.

In contrast, the smoothed-terrain experiment (**Figure 6(b)**) displayed a more uniform 850 hPa wind field at the same time, with no apparent convergence center near the storm core, preventing the organization of strong upward motion and rainfall at 20:00.

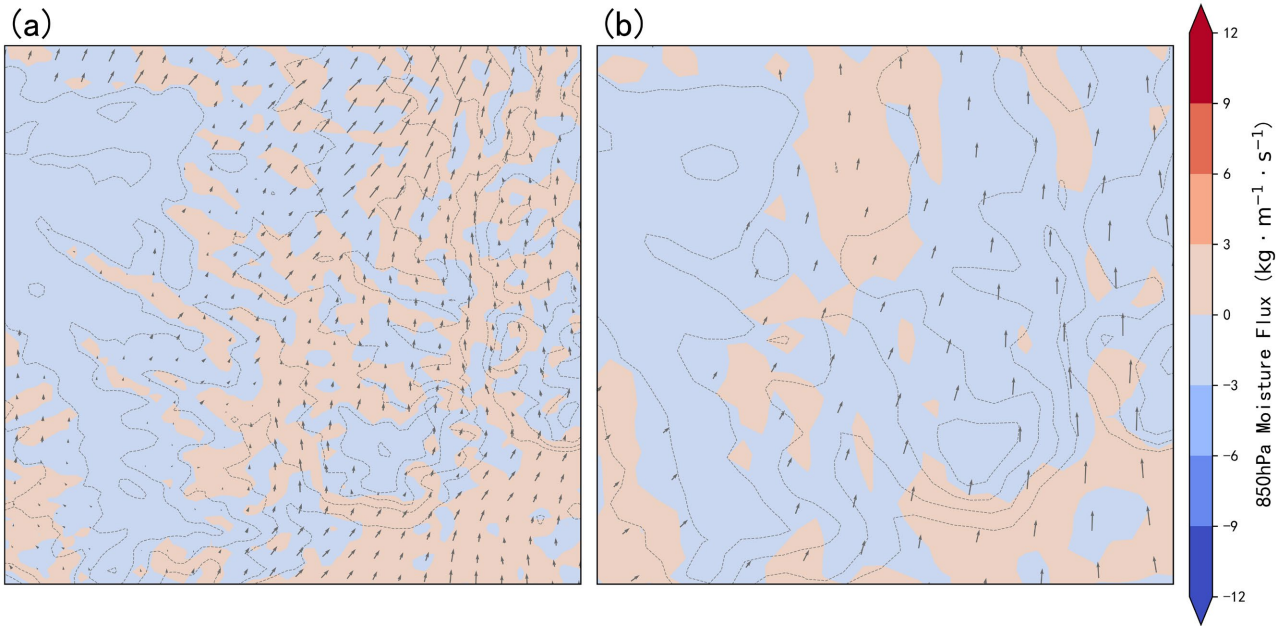

Figure 6. Distribution of 850 hPa wind field, moisture flux ($kg \cdot m^{-1} \cdot s^{-1}$), and Convective Available Potential Energy (J/kg): (a) Real-terrain experiment; (b) Smoothed-terrain experiment. The background shading represents the intensity of moisture flux, and the contours denote CAPE values.

The distribution of CAPE further validates the terrain-triggered convection process. At 20:00, a local high-CAPE region (1200 J/kg) appeared near Yan'an in the real-terrain simulation, whereas CAPE values in the smoothed-terrain case remained generally below 800 J/kg and spatially homogeneous. As the terrain-induced uplift allowed air parcels to reach the level of free convection, CAPE in the real-terrain case rapidly decreased by 21:00, indicating active energy release and convection initiation. In contrast, in the smoothed-terrain simulation, CAPE consumption did not occur until after 22:00. This temporal lag corresponds precisely to the delay in precipitation onset, confirming that the hilly terrain facilitated earlier conversion of convective instability into kinetic energy.

4.3. Evolution and Merging of Convective Cells

Simulation results show that the hilly terrain of the Loess Plateau not only triggered multiple convective cells but also influenced their subsequent movement and merging, ultimately leading to the formation of extreme precipitation. To analyze this merging and intensification process, the evolution of convective cloud clusters was examined using the simulated radar reflectivity at 2 km height, which effectively represents the position and strength of convective clouds.

In the real-terrain experiment, by 21:00, three major convective cells—labeled C1, C2, and C3—had formed over adjacent hilltops (**Figure 7(a)**). The locations of these cells closely coincided with the previously identified low-level convergence centers. Between 21:00 and 22:00, C1 and C2 moved northward and gradually approached each other, while a western cell (C4) was advected southeastward by the northwesterly flow, converging toward the same region. By around 22:30,

these previously isolated convective cells merged into a single, organized strong-echo region (C5, Figure 7(b)).

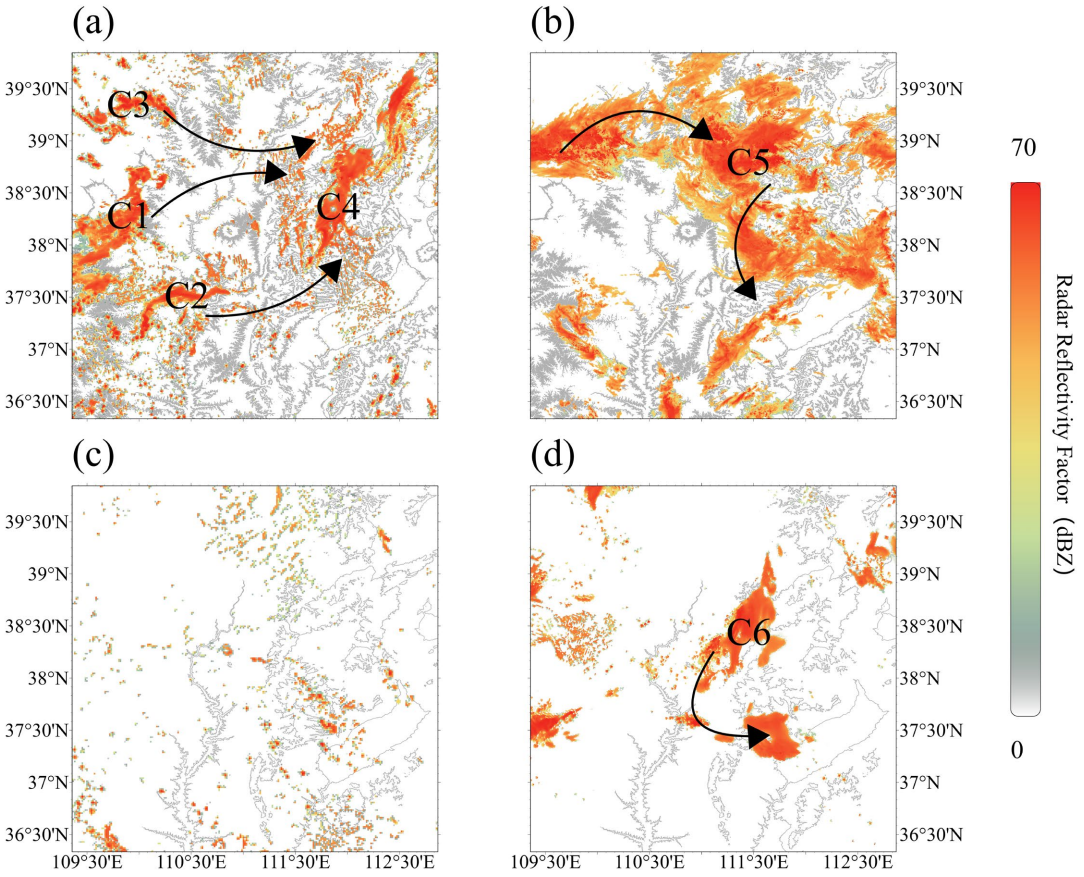

Figure 7. Simulated radar reflectivity factor (dBZ) at 2 km altitude and convective cell locations in the real-terrain experiment: (a) Real terrain, 21:00 BT 15 July 2022; (b) Smoothed terrain, 21:00 BT 15 July 2022; (c) Real terrain, 22:30 BT 15 July 2022; (d) Smoothed terrain, 22:30 BT 15 July 2022. The labeled C1, C2, and C3 denote major convective cells, and black arrows indicate their movement directions and merging trends.

The merged convective system exhibited a broader cloud top, a stronger reflectivity core, and deeper vertical development. At this time, surface rain gauges recorded a sharp increase in hourly rainfall, with several stations in Ansai and Zizhou reporting hourly intensities exceeding 54.2 mm·h^{-1}. This clearly indicates that the merging of convective clouds enhanced precipitation efficiency and expanded the rainfall coverage. The merged mesoscale convective system persisted for 1 - 2 hours, gradually moving southeastward while weakening and dissipating. By the early morning of July 16, the main rainband had shifted out of the study area.

In contrast, the smoothed-terrain experiment produced scattered and weaker convective cells. It was not until 22:00 that two or three small, isolated reflectivity cores appeared near the center of the domain. These cells remained widely separated and failed to merge effectively, dissipating individually soon after. This explains the absence of a persistent heavy-rainfall region in the smoothed-terrain case: without terrain-induced organization and multi-cell merging, the contribu-

tion of any single convective cell was limited and short-lived. Consequently, the terrain acted as an "organizer" in this event—hilly topography not only triggered multiple convective cells but also guided airflow patterns, influencing cell movement paths and promoting their aggregation.

To quantitatively evaluate the impact of cell merging on rainfall enhancement, the mean rainfall intensity and area of heavy precipitation were compared before and after merging. Between 21:00 and 22:00, the area with rainfall intensity ≥ 20 mm/h in the main storm region expanded from 243.5 km^2 to 498.6 km^2, an increase of about 2.1 times, while the mean rainfall intensity rose from 15.6 mm/h to 39.2 mm/h. During the merging period (21:30-22:30), the precipitation efficiency per unit area increased by approximately 57.2%. In this case, the terrain-triggered generation and rapid merging of multiple convective cells were clearly the core mechanisms responsible for the sharp intensification of rainfall.

Synthesizing the above results, a closed physical chain can be established to describe how hilly terrain influences extreme precipitation: Moist and warm airflow transported along the periphery of the subtropical high encounters the hilly terrain of the Loess Plateau, where it is forced to ascend, forming orographic convergence lines and updraft zones. Multiple localized lifting centers trigger the formation of convective cells, with each hilltop acting as a potential rainfall focus. Under the influence of low-level wind fields, these convective cells move toward the convergence zone and merge, accompanied by intense secondary circulations and release of convective instability energy, rapidly amplifying rainfall intensity. Ultimately, the merging of multiple cells into a mesoscale convective system (MCS) produces regional-scale extreme precipitation.

5. Discussion

Several limitations and uncertainties remain in this study. First, numerical simulations inherently contain biases. For instance, the simulated location of the rainfall center was approximately 20 km north of the observation, likely due to errors in the initial field or limitations in the physical parameterization schemes. Although sensitivity experiments confirmed the qualitative role of topography, the quantitative magnitude of its impact is still influenced by the model resolution [24].

Second, the absence of data assimilation may have caused timing deviations in convective initiation. For example, in the real-terrain simulation, convection was triggered around 21:00, whereas in reality, strong radar echoes were already observed near 20:00. While this discrepancy does not alter the underlying mechanism of terrain-induced convection, a 1-hour difference can be crucial for operational forecasting [25]. Future work could incorporate radar reflectivity assimilation to improve the timing accuracy of convection initiation and enhance forecast reliability. This 1-hour timing lag likely delayed the merger of convective cells and slightly weakened the simulated hourly rainfall peak.

Third, the smoothed-terrain experiment represents an idealized extreme scenario, since the Loess Plateau in reality is never perfectly flat. Therefore, the dif-

ference between the real and smoothed simulations can be regarded as an upper-bound estimate of terrain effects. In actual conditions, partial terrain flattening may reduce rainfall to some extent but not as drastically as in the fully smoothed case. Nevertheless, this idealized design provides a valuable conceptual contrast, serving as a controlled framework for quantifying the magnitude of terrain influence [26].

Despite these limitations, this study offers new insights into the mechanisms of heavy rainfall in the hilly-gully region of the Loess Plateau. It demonstrates that rainstorms in such terrain differ fundamentally from those over plains: multiple convective cells tend to initiate nearly simultaneously over individual hills and then merge rapidly within a short period. This multi-point convective organization contrasts with the more common linear squall lines or isolated supercells observed elsewhere. Consequently, forecasting in similar terrains should not rely on a single triggering condition. Identifying multiple potential convective initiation zones based on terrain features could improve forecast accuracy. Moreover, dynamically adjusting terrain smoothing levels in numerical models—while maintaining stability—may allow models to resolve more realistic convective cells, thereby reducing missed events.

6. Conclusions

The results of this study demonstrate that the complex terrain of the central Loess Plateau effectively triggers and organizes multiple convective cells by enhancing low-level airflow convergence and promoting orographic lifting. These convective cells subsequently merge under the influence of low-level wind fields, forming a mesoscale convective system (MCS) that substantially amplifies rainfall intensity.

Specifically, in the real-terrain experiment, the maximum accumulated precipitation at the storm center reached 152.8 mm, more than double that of the smoothed-terrain case (74.6 mm). The difference in rainfall intensity was also pronounced: the peak hourly rainfall reached 50 mm/h under real terrain but only 10 mm/h with smoothed terrain. During the merging phase, both the intensity and area of heavy rainfall expanded markedly—between 21:00 and 22:00, the area with rainfall intensity ≥ 20 mm/h increased from 243.5 km^2 to 498.6 km^2, while the mean rainfall intensity rose from 15 mm/h to 40 mm/h.

These findings indicate that the hilly terrain of the Loess Plateau not only serves as the generation zone for convective cells but also facilitates their subsequent merging, ultimately leading to the occurrence of regional-scale extreme precipitation events.

Conflicts of Interest

The authors declare no conflicts of interest regarding the publication of this paper.

References

[1] Liu, H., Ma, X. and Liang, S. (2021) Analysis of β-Mesoscale Characteristics of Local

Torrential Rain in Northern Shaanxi on 25 July 2017. *Torrential Rain and Disasters*, **40**, 374-382. (In Chinese)

[2] Zhang, Q., Tao, S. and Peng, J. (2008) Advances in Studies on Mechanisms of Disastrous Weather and Climate Events in China. *Chinese Journal of Atmospheric Sciences*, **32**, 815-825. (In Chinese)

[3] Ding, Y., Ren, G., Shi, G. (2007) National Assessment Report on Climate Change (I): Historical and Future Trends of Climate Change in China. *Advances in Climate Change Research*, **3**, 1-5. (In Chinese)

[4] Fu, S.M., Deng, Z.F. and Wang, X.M. (2013) Mesoscale Structure and Evolution of a Heavy Rainfall Event Associated with a Vortex over Northern China. *Acta Meteorologica Sinica*, **71**, 234-250. (In Chinese)

[5] Zhang, H., Chen, W. and Sun, W. (2006) Analysis of a Heavy Rainfall Event in Northern Shaanxi Influenced by a Typhoon and the Hetao Vortex. *Plateau Meteorology*, **25**, 52-59. (In Chinese)

[6] Wang, W., Li, Z. and Xu, Q. (2009) Radar Echo Characteristics of Heavy Rain Associated with a Low Vortex. *Meteorological Science and Technology*, **37**, 533-537. (In Chinese)

[7] Liang, F. and Tao, S. (2007) Analysis of Rainstorm Process during the Development of the Hetao Cyclone in July 1998. *Journal of Applied Meteorological Science*, **18**, 577-585. (In Chinese)

[8] Jiang, X.M., Yuan, H.L., Xue, M., Chen, X. and Tan, X.G. (2014) Analysis of a Torrential Rainfall Event over Beijing on 21-22 July 2012 Based on High-Resolution Model Analyses and Forecasts. *Acta Meteorologica Sinica*, **72**, 207-219. (In Chinese)

[9] Liu, Y., Wang, C. and Wang, N. (2006) Role of Low-Level Jet in Heavy Rainfall over the Loess Plateau. *Shaanxi Meteorology*, **5**, 1-4. (In Chinese)

[10] Du, Y., Chen, G., Han, B., Mai, C., Bai, L. and Li, M. (2020) Convection Initiation and Growth at the Coast of South China. Part I: Effect of the Marine Boundary-Layer Jet. *Monthly Weather Review*, **148**, 3847-3869. https://doi.org/10.1175/MWR-D-20-0089.1

[11] Zhang, F., Li, G. and Yue, J. (2019) The Moisture Sources and Transport Processes for a Sudden Rainstorm Associated with Double Low-Level Jets in the Northeast Sichuan Basin of China. *Atmosphere*, **10**, Article 160. https://doi.org/10.3390/atmos10030160

[12] Liu, H., He, M. and Wang, B. (2014) Review and Prospect of Research on Low-Level Jets. *Acta Meteorologica Sinica*, **72**, 191-205. (In Chinese)

[13] Wang, H., Luo, Y. and Jou, B.J.-D. (2014) Initiation, Maintenance, and Properties of Convection in an Extreme Rainfall Event during SCMREX: Observational Analysis. *Journal of Geophysical Research: Atmospheres*, **119**, 13,206-13,232. https://doi.org/10.1002/2014JD022339

[14] Schumacher, R.S. and Johnson, R.H. (2006) Characteristics of U.S. Extreme Rain Events during 1999-2003. *Weather and Forecasting*, **21**, 69-85. https://doi.org/10.1175/WAF900.1

[15] Jing, X., Li, Q. and Tu, N. (2013) Characteristics and Causes of a β-Mesoscale Sudden Rainstorm over the Loess Plateau. *Torrential Rain and Disasters*, **32**, 242-248. (In Chinese)

[16] Liu, L. and Liu, X. (2011) Evolution of Landscape Pattern and Ecosystem Service Function on the Loess Plateau. *Journal of Arid Land Resources and Environment*, **25**, 8-13. (In Chinese)

[17] Zhang, Y. and Zhu, Q. (2006) Characteristics of Erosive Rainfall on the Loess Plateau. *Journal of Arid Land Resources and Environment*, **20**, 99-103. (In Chinese)

[18] Gao, X., Miao, J. and Guo, X. (2017) Simulation of Heavy Rainfall over the Loess Plateau Using the WRF Model. *Meteorology*, **43**, 1341-1351. (In Chinese)

[19] Nishikawa, M., Hiyama, T., Tsuboki, K. and Fukushima, Y. (2009) Numerical Simulations of Local Circulation and Cumulus Generation over the Loess Plateau, China. *Journal of Applied Meteorology and Climatology*, **48**, 849-862. https://doi.org/10.1175/2008JAMC2041.1

[20] Muñoz-Sabater, J., Dutra, E., Agustí-Panareda, A., Albergel, C., Arduini, G., Balsamo, G., *et al.* (2021) ERA5-Land: A State-Of-The-Art Global Reanalysis Dataset for Land Applications. *Earth System Science Data*, **13**, 4349-4383. https://doi.org/10.5194/essd-13-4349-2021

[21] Huang, H. and Ni, Y. (2004) Numerical Experiment of Terrain Replacement. *Acta Meteorologica Sinica*, **62**, 76-87. (In Chinese)

[22] Banacos, P.C. and Schultz, D.M. (2005) The Use of Moisture Flux Convergence in Forecasting Convective Initiation: Historical and Operational Perspectives. *Weather and Forecasting*, **20**, 351-366. https://doi.org/10.1175/WAF858.1

[23] Huang, Y., Qin, D. and Qiu, X. (2012) Convective Cloud Merger during Rainstorms. *Chinese Journal of Atmospheric Sciences*, **36**, 1135-1149. (In Chinese)

[24] Kirshbaum, D.J. and Durran, D.R. (2004) Factors Governing Cellular Convection in Orographic Precipitation. *Journal of the Atmospheric Sciences*, **61**, 682-698. https://doi.org/10.1175/1520-0469(2004)061<0682:fgccio>2.0.co;2

[25] Houze, R.A. (2004) Mesoscale Convective Systems. *Reviews of Geophysics*, **42**, RG4003. https://doi.org/10.1029/2004RG000150

[26] Fu, D. and Guo, X. (2007) Role of Cumulus Merger in Convective Systems. *Chinese Journal of Atmospheric Sciences*, **31**, 635-644. (In Chinese)